VDMA
Fluid Power Association

23rd ISC

International Sealing Conference

Stuttgart, Germany
Sept.30 - Oct.1, 2026

Sealing the future –
Facing the challenges of tomorrow

UNI STUTTGART

Fachverband Fluidtechnik im VDMA e. V. Lyoner Str. 18
50628 Frankfurt am Main
Germany

Phone +49 69 6603-1513
E-Mail maximilian.baxmann@vdma.eu

Internet www.vdma.eu/fluid

Rethinking Thermal Contact Analysis of PTFE Rotary Lip Seals: A Simplified, Physics-Based Approach

Mirco Gronitzki, Sarah Shabbir

Failing of radial shaft seals at high speeds is often related to thermal stress in the sealing contact. Seal materials as well as sealed fluids can be impacted. Contact temperatures thus have been the scope of various experimental or theoretical studies in the past. They often result in challenging measurements and/or complex thermal networks.

Saint-Gobain has re-thought this problem and approached it from a deliberately simplified yet precise perspective. The presented work is based on an extensive experimental campaign, in which numerous measurements were conducted to identify key influences and assess their repeatability. Special attention was given to the interpretation and measurement technique for capturing local temperature gradients, which can complicate contact temperature measurements. Based on this, a Heat Transfer Finite Element Model was developed and verified step by step. An analogy model was used in parallel to foster insights and to reduce the thermal problem to its dominant mechanisms.

The combined approach leads to a practical understanding of the key parameters influencing contact temperature evolution. The results demonstrate that a simplified, well-calibrated framework can deliver precise and actionable insights into high-speed seal thermal behaviour.

1 Introduction

PTFE rotary lip seals (RLS) are dynamic contacting seals that slide over a rotating shaft, occupying a specific operating niche between elastomeric lip seals and mechanical face seals. As is characteristic for such seals, numerous failure mechanisms are related to the contact temperature.

The operating environments for this class of seals are varied and vast, spanning multiple market segments including aerospace, automotive, space and industrial compressors. Such systems require shaft sealing, and PTFE RLS accordingly serve turbopumps, vacuum pumps, gearboxes and turbines here. Whilst the speed requirements of these systems differ considerably, so too do the expectations on efficiency, leakage performance and service life. Nevertheless, the common denominator across all dynamic high-speed RLS applications is a three-part sealing system: the seal, the shaft and the sealed fluid. All three components must be capable of withstanding the contact temperatures generated at the interface where the seal runs against the shaft, Figure 1.

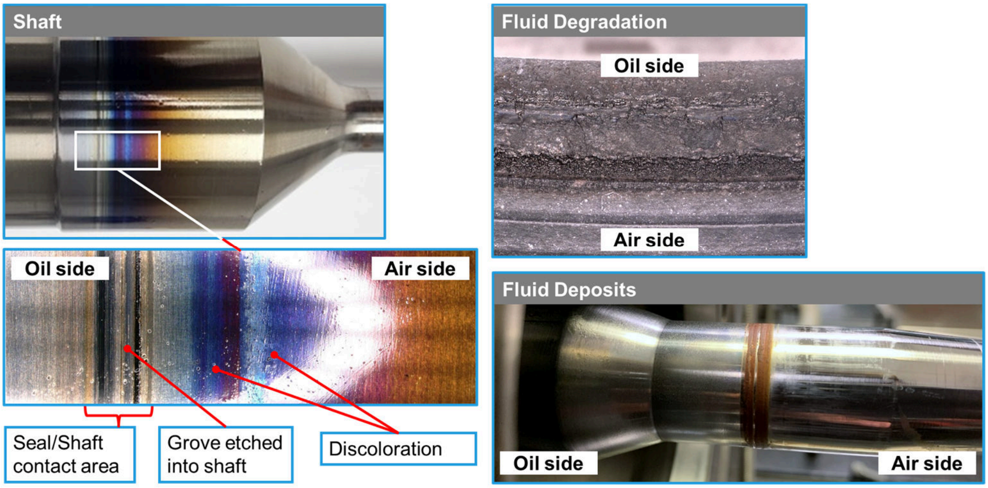

Figure 1: Temperature related failure patterns of rotary lip seals

The sump temperature, T_0, represents the system baseline. The total maximum temperature at the local interface, T_C, is expressed as the sum of the sump temperature and the additional temperature rise ΔT arising from frictional heat generated by rotation:

$$T_C = T_0 + \Delta T \tag{1}$$

Determination of T_C for a given system is necessary to establish whether it will exceed the maximum operating temperature of either the sealing material or the sealed fluid. Notably, the shaft is typically the last component to be thermally compromised and sealed oils frequently degrade at temperatures below those tolerated by the PTFE lip material itself.

The ability to assess whether a design is approaching a critical threshold and is likely to fail is of growing importance as application speed requirements become increasingly demanding. The thermal model developed here therefore serves two distinct purposes: to predict the contact temperature for a given system configuration, enabling seal designs to be assessed against an appropriate safety margin; and to evaluate the sensitivity of that temperature to changes in system variables including shaft geometry, coating thermal conductivity, or the presence of an air gap beneath the contact zone from a poorly press-fitted sleeve, etc. This second capability provides direct insight into how geometrical and material factors alter the local thermal resistance and, consequently, the rate of heat dissipation at the interface.

The problem, however, is not straightforward. There is a wide range of seal materials, and an effectively infinite number of design variations that produce a given radial load and a wide range of achievable radial loads too. Furthermore, most applications involve complex duty cycles of speed, pressure and temperature, all of which influence the temperatures generated at the local interface.

Whilst the heat generated at the contact is the primary factor in determining T_C, it cannot be considered in isolation. The heat dissipated from the interface, Q_T, is equally consequential, and is governed by the thermal resistances, R_T, of the surrounding system. These resistances depend on parameters such as shaft geometry, shaft material thermal properties, system architecture, the fluid being sealed, and its fill level, among others. In the present work, R_{T_RHS} denotes the thermal resistance on the air side of the seal (the backside), whilst R_{T_LHS} denotes the thermal resistance on the fluid side (the frontside). These denote the two main heat dissipation paths possible.

Determining both the heat generated at the seal interface and the heat dissipated into the surrounding system is the basis upon which the maximum contact temperature can be resolved. This requires a degree of system simplification through considered assumptions, the lumping of thermal resistances, and the identification of which resistances remain effectively constant under given operating conditions as it is not practicable to account for every possible configuration or variation.

The approach adopted here combines experimental testing with thermal simulation. Testing alone, whilst the most accurate means of measurement, is costly, repetitive, and impractical as a general-purpose tool. Simulation alone lacks the grounding or data to be reliable or yield meaningful predictive insight. The combined approach enables precise calibration of the thermal model against highly repeatable measurements, supports verification across multiple systems, and provides the capability to predict contact temperatures to an accuracy sufficient for the purposes of seal design and qualification. For both to be valid, the measurement technique must be robust and produce datasets that are repeatable and consistent whilst the thermal model must be calibrated and set up in a manner that is the closest representation to reality without overcomplicating or oversimplifying the system. This is addressed in the methodology, section 3, of this paper.

The sections that follow review the existing literature on contact temperature measurement and thermal modelling relevant to this field, upon which the present work builds. A detailed methodology section then describes both the experimental programme and the thermal model developed. Results are subsequently presented and discussed, and the paper closes with a summary of key conclusions.

2 Background

A brief review of the literature in the two focus areas of this study is presented below. The review traces the evolution of prior research, highlighting key developments and establishing the fundamental foundation upon which the present work is built.

2.1 Contact Temperature Measurements

Contact temperature measurements on dynamic seals have been investigated in various practical studies. As early as 1966, Lines et al. [10] embedded a miniature thermocouple in the shaft surface, which was fixed and thermally insulated from the surrounding material using an adhesive. This approach was refined by Wollesen [17], who prepared the thermocouple within a separate cartridge. The cartridge was subsequently press-fitted into the shaft and finished by grinding, ensuring smooth integration with the surface. This step in particular has raised the level of the detected temperatures significantly. A temperature profile along the sealing lip was obtained by repositioning the test shaft. He also demonstrated that the applied insulation does not result in any significant measurement error.

This technique was later adopted by Engelke [3], Wennehorst [16], and other researchers in combination with state of the art telemetry signal transducers, although in some cases the cartridge was omitted. Using these methods, measured temperature increases ΔT ranged from 5 to 60 K, depending on factors such as the test specimen, shaft diameter, and operating conditions. However, several studies report that this approach is not viable for long-term investigations due to the limited durability of the integrated shaft sensors. Thus, it was generally not feasible to scan larger data arrays or verify repeatability.

For his investigations on PTFE radial shaft seals, Bock [1] likewise applied miniature thermocouples; however, these were embedded in the sealing lip rather than in the shaft surface. Consequently, the sensors are inherently positioned closer to the air side of the seal and do not consistently remain in direct contact with the lubricant.

In publications by IMA [4], [6], thermographic cameras are often used to monitor the shaft or seal ring surface on the air side of the system. Under these conditions, the measurement spot is typically separated from the actual sealing interface of PTFE shaft seals by several millimetres. In some cases, this circumstance was compensated for by an additional offset.

2.2 Thermal Networks and Modelling

Thermal modelling of rotary lip seals has evolved considerably over time, with successive contributions progressively increasing the fidelity of the thermal resistance network used to describe the seal-shaft-fluid system.

The earliest formal thermal model presented here for RLS was introduced by Upper (1967) [15], who proposed an electric-circuit analogy with approximately three lumped thermal resistances representing the lip, fluid film and shaft. This foundational framework established the structure upon which subsequent models were built. Stakenborg & van Ostayen (1989) [13] advanced this by incorporating finite element method (FEM) stress and thermal network analysis, expanding the resistance count to approximately four to five resistances, adding contributions from the sealing contact zone, rubber body, shaft, housing and ambient.

Kang & Sadeghi [9] introduced a multigrid finite-difference thermal Reynolds solver coupled with energy equations, resolving approximately four resistances across the fluid film, lip, shaft and side-leakage path. Day & Salant [2] presented the first fully coupled thermo-elastohydrodynamic (TEHD) model with temperature-dependent viscosity and elastic modulus, extending the network to approximately six resistances by accounting for asperity contact, the fluid film, rubber deformation, garter spring, air-side convection and the shaft. Hajjam & Bonneau [6] further refined this by introducing a roughness micro-layer and a thermoelastic lip formulation within a FEM-TEHD framework, reaching approximately seven resistances with both local and global temperature approaches.

Maoui et al. [11] incorporated three-dimensional non-axisymmetric elastomeric deformations within a fully coupled fluid-thermal-structural model at approximately eight resistances. Feldmeth et al. [4] introduced a three-scale CFD/FEM approach spanning macro, meso and micro sub-models with ten resistances. More recent contributions have moved towards transient and mixed-lubrication regimes: Thielen (2019) [14] developed a transient TEHD model coupling the Reynolds equation, energy equation and Boussinesq elasticity at approximately four resistances. Huang et al. [8] addressed mixed lubrication with viscosity-temperature coupling and convective heat transfer at approximately seven resistances; and Nomikos et al. [12] presented a semi-analytical model validated on a vehicle test-rig, incorporating approximately nine resistances spanning the contact, shaft, sump, housing and ambient.

The literature reveals several important trends. First, the use of thermal network models to represent sealing systems is well established and is not a novel concept. Over time, these models have evolved toward greater accuracy, albeit sometimes at the cost of increased complexity. They have been investigated under a wide range of boundary conditions and modelling assumptions. Second, the simplification of thermal networks through the aggregation of individual thermal resistances into broader categories has been employed previously [14] as a means of reducing model complexity while retaining predictive capability. This approach forms a key foundation upon which the present work builds. Finally, the literature consistently demonstrates the importance of accurate thermal prediction for understanding seal behaviour, improving seal design, and extending the operating limits of contacting sealing technologies, a challenge that underlines the motivation of this investigation.

Despite these advances, there remains a comparatively unexplored area with a lack of experimentally verified, simplified thermal models that are both calibrated against high-quality measurements and assessed across a range of seal geometries and working fluids. The reliability of such models depends critically on the quality and robustness of the experimental data used for calibration. In particular, the development of accurate and repeatable measurement techniques remains a significant challenge. Addressing this gap is the primary objective of the present study.

3 Methodology

The methodology is structured around two areas: experimental testing and thermal modelling. The experimental work centres on a test setup employing a novel measurement approach, the details of which are described in section 3.1. The thermal model, developed in parallel and calibrated against the experimental outputs, is described in section 3.2.

3.1 Experiments: Temperature Measurement and Optimization

3.1.1 Test Equipment

For investigation on dynamic seals Saint-Gobain Omniseal solutions uses a range of test rigs. These can be categorized as functional and endurance test rigs:

- Functional test rigs ➔ scientific investigation
  Generate deep understanding of how seals work or fail
- Endurance test rigs ➔ lifetime tests and product verification

The studies presented here were primarily conducted using the functional test rig shown in Figure 2. This enables the testing of dynamic shaft seals at speeds of up to 32,000 rpm, while varying pressure, temperature and media.

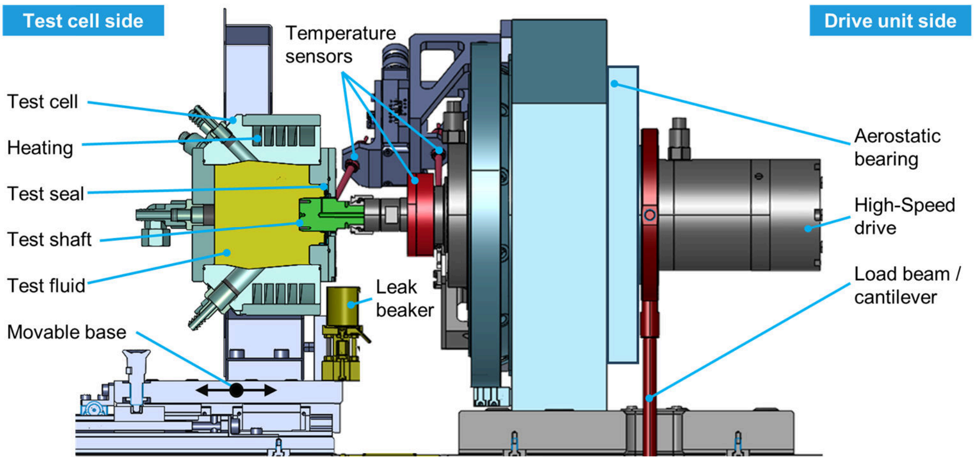

Figure 2: Saint-Gobain High-Speed Test Rig “SoS I”

Two aspects are of particular interest for the present work: friction losses and the temperatures at and around the sealing contact. For the first aspect the rig is equipped with a highly precise friction torque measurement system, featuring an air-bearing unit integrated surrounding the drive and a temperature-insensitive, almost drift-free radial force support.

The drive is directly connected to the test shaft, which extends into the opposite test cell. This keeps the test cell side free of sensitive sensors and ensures robust operation. The test cell can be equipped on one side with a transparent cover, allowing direct observation of the oil distribution inside. Seeing things can sometimes be as helpful as the most complex measurements.

For the second aspect, the setup includes multiple sensors for temperature measurement. The sump temperature is monitored using thermocouples located within the test cell. Furthermore, several infrared ($T_{IR,\ 1\text{-}3}$) spot temperature sensors enable non-contact measurement of the temperature distribution along the shaft (Figure 3).

As described by Wollesen, Engelke, Wennehorst and others, a thermocouple is also integrated directly into the test shaft, with its signal transmitted contactless to the stationary part of the test rig. Moreover, the test cell containing the specimen can be axially displaced during operation, allowing the temperature profile along the sealing interface to be scanned. The sensor is labelled as T_{M1} in the following figures and diagrams. If positioned at the temperature peak underneath the lip it should represent the max. contact temperature T_C.

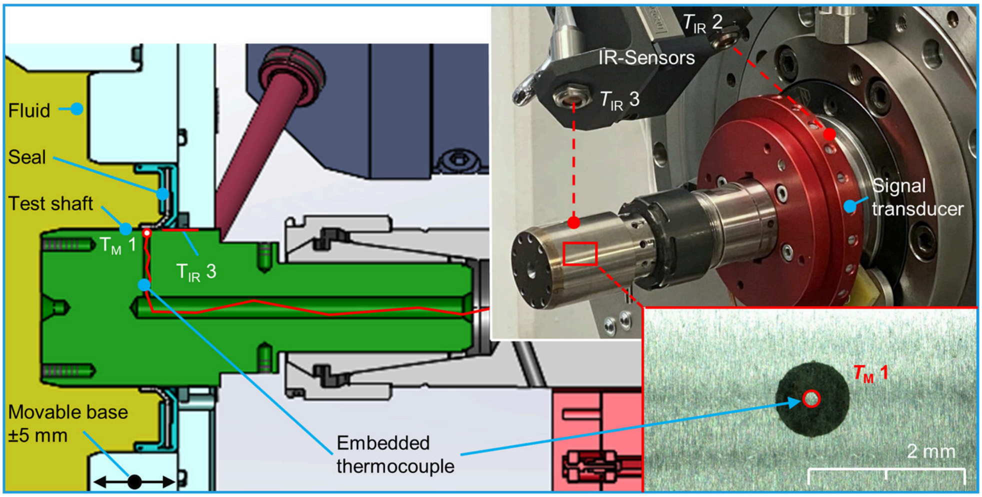

Figure 3: Shaft temperature measurement setup

Particular attention was given to the sensor preparation. A type J thermocouple with a diameter of approximately 0.3 mm was installed in a 0.8 mm bore. The embedding material consists of filled polyimide (PI) and is resistant up to around 300 °C. The thermocouple is positioned as centrally as possible within the bore, and about 50% of its height is removed during the final machining of the shaft surface. This procedure creates a small, surface-focussed measurement point.

3.1.2 Initial measurements

To gain initial experience with the system, large test campaigns were conducted. Rotational speed, pressures, and fill levels were varied, utilizing elastomer- and PTFE-based seals in the 30 to 60 mm range. Figure 4 shows a representative surface temperature scan used to determine the location of the peak temperature, as well as selected results from the initial measurement campaign. While the results offered a good indication of the anticipated temperature range, they were not satisfactory in terms of their scatter and repeatability.

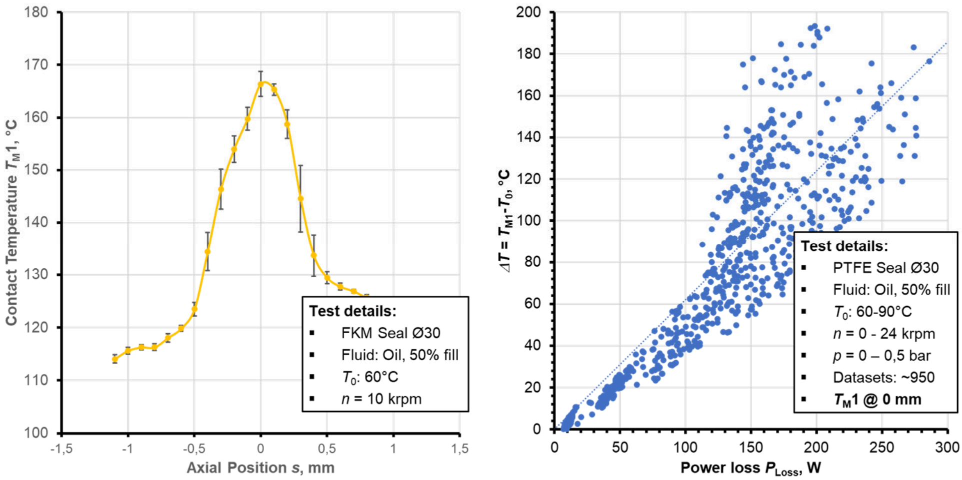

Figure 4: Contact temperature scan (left side), initial measurements (right side)

3.1.3 Optimization

Initial improvements were achieved by introducing a holding time of at least 30 minutes at each set of test parameters to ensure sufficient thermal stability of the system. It was also found that parameter sets with changing pressure loads are not beneficial, as they cause axial displacements of the sealing lip on the shaft and thus affect the positioning of the sensor.

These initial adjustments improved the measurements but were not sufficient to reduce the scatter to an acceptable level. The key solution was identified through the analysis of multiple temperature scans and the simulations described in section 3.2.2. These showed a significant temperature gradient near the seal contact, where even minor positioning deviations can significantly influence the measured values.

Relocating the measurement point slightly outside the seal contact area substantially reduces measurement scatter. In addition, the thermocouple is no longer subject to wear from direct seal contact. Positioning the measurement point on the oil side is preferable to the air side, as the typical PTFE seal contact profile requires considerably less displacement in that direction. Figure 5 shows the final setup used for the subsequent measurements.

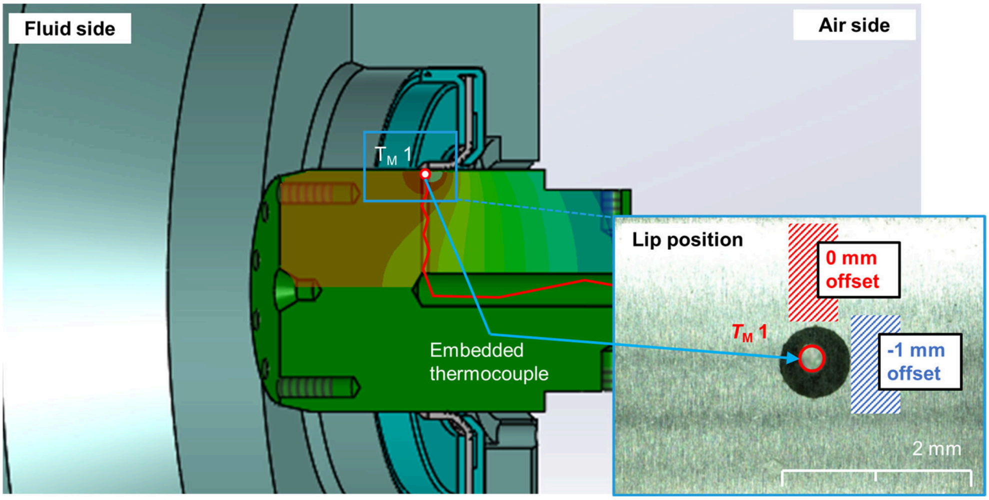

Figure 5: Optimized shaft sensor setup with temperature field overlay

The implemented setup led to a significant reduction in measurement scatter. As a matter of course, the offset position of the sensor must be taken into account during the subsequent comparison with the simulation. Figure 6 shows a representative measurement involving multiple seals and shafts, together with a reverse-transformation of the measured values T_{m1} @-1mm-position to the corresponding contact temperature T_C.

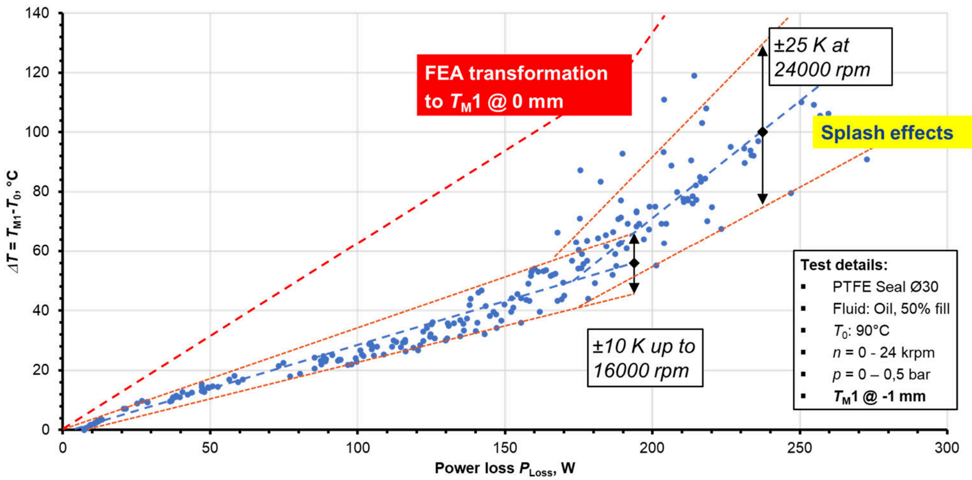

Figure 6: Measurement example with optimized setup

Up to 16000 rpm (~25 m/s), the spread is significantly reduced. A nearly linear relationship of P_{Loss} and ΔT is observed. At higher rotational speeds, both the slope and as well the measurement spread change. When a hollow shaft configuration is used instead of a solid shaft for the tests, the observed effect largely disappears. It's therefore assumed that the observed effect is primarily caused by splash effects and eliminated in the case of the hollow shaft configuration at the fluid is forced to the surface by the applied centrifugal forces.

More experimental studies with various setup variants are shown in Figure 7. These were used to calibrate and verify the model described in the following section.

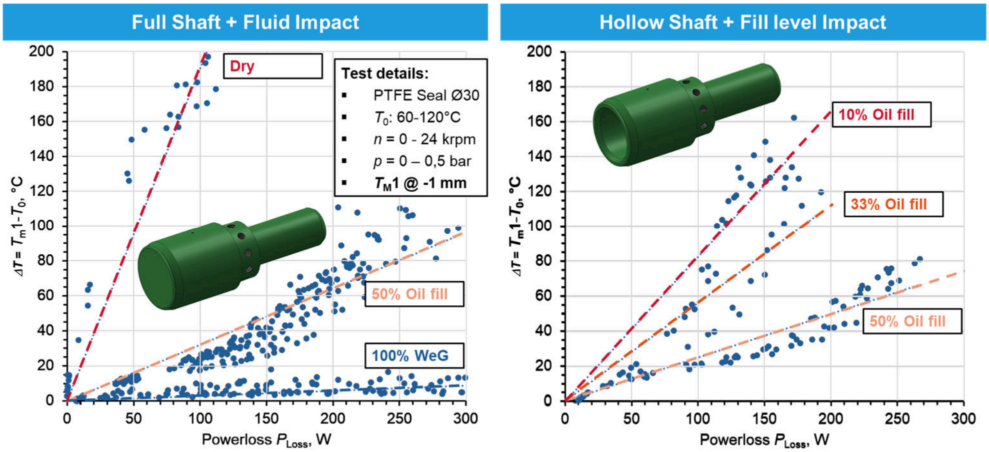

Figure 7: Variants with different media, fill levels, and shaft geometries

3.2 Simulation: Thermal Model Calibration and tuning

3.2.1 Model Setup

The thermal model is developed in ABAQUS using the built-in Heat Transfer solver, which resolves the energy equation across the model domain by computing nodal temperatures iteratively until equilibrium is reached. The solver accounts for conduction and convection heat transfer and is well established for steady-state thermal problems of this nature.

The model geometry, dimensions, boundary conditions and material assignments are defined to replicate the SoS I test rig described in Section 3.1, including the relevant contact interfaces, thermal insulations and component connections. This test rig, serving as the fundamental reference system, provides direct local interface temperature measurements, T_C which are used for model verification. The resulting FEA geometry and setup are shown in Figure 8.

3.2.2 Temperature Equation

Following equation (1) above, the ΔT can be further described in equation (2) as follows

$$T_C = T_0 + f(\mu.\pi.n.F_R.d, R_{T\,SYSTEM}) \tag{2}$$

The induced power into the system is a function of the following parameters and are usually a variable of the operational conditions like speed, temperatures and pressures.

$\mu = coeficient\ of\ friction, F_R = Seal\ Radial\ Load\ and\ d = shaft\ diameter$

Thus, knowledge of the induced power in the system, the initial sump temperature and the thermal resistance of the system enables prediction of the final contact temperature at the local interface. Determining the induced power and the initial sump temperature is relatively straightforward; the same cannot be said for the thermal resistance of the system.

3.2.3 Thermal Resistances

When heat is generated at the local interface, three principal dissipation paths exist: through the seal, along the shaft towards the fluid side, and along the shaft towards the air side. Given that:

$$R_T = \frac{l}{kA} \tag{3}$$

the thermal resistance of a polymer sealing lip can be approximately three orders of magnitude greater than that of the shaft for comparable geometries due to the very low thermal conductivity of those materials. The seal lip therefore acts effectively as a thermal insulator, and heat dissipation in that direction is taken as negligible. This constitutes the first assumption in determining the resistances.

The metallic shaft, by contrast, presents a low thermal resistance and conducts heat efficiently along its length. Heat dissipation is therefore governed by the shaft, travelling in either direction away from the interface. As introduced in Section 1, $R_{T\,RHS}$ & $R_{T\,LHS}$ denote the thermal resistances on the air side and fluid side of the seal respectively. In each case, multiple individual resistances are lumped into a single representative value to reduce model complexity without loss of physical relevance.

On the air side (RHS), the shaft is connected to a thermal fixture held at ambient temperature, establishing a defined temperature gradient along the exposed shaft length. Air convection around the shaft also contributes to this resistance. Both factors remain effectively constant for this given system, and $R_{T\,RHS}$ is therefore treated as fixed. This constitutes the second assumption.

On the fluid side (LHS), the situation is considerably more complex. The shaft is exposed to the sump or chamber, which may be filled with fluid to varying levels, flooded with oil mist, or running dry entirely. The shaft itself may be solid or hollow, directly affecting how efficiently circulating fluid can cool it. Coatings of varying thickness and thermal conductivity further modify the local resistance. In many applications, the seal runs on a sleeve which may have an imperfect press fit to the shaft, introducing contact resistance. The presence of a spline or similar geometric feature beneath the seal can create localised air gaps in the immediate vicinity of the heat source, effectively thermally isolating the shaft and trapping heat at the interface –

all of which frequently drive thermally-driven failures. It is for these reasons that $R_{T\,LHS}$ is the dominant variable that changes significantly from test to test, altering the thermal resistance of the system and determining the direction of heat flow.

It should be noted, however, that a constant $R_{T\,RHS}$ does not imply that the air side remains cooler than the fluid side under all conditions. In oil or water-cooled applications, the temperature distribution typically reveals higher temperatures on the air side, as the direction of net heat transport is governed by the relative magnitude of the resistances on each side. In dry-running applications, the reverse is observed: the fluid side reaches higher temperatures, as is depicted in the case study shown in Figure 8.

The electrical analogy model that this is based on is depicted in Figure 9. In this framework, temperature corresponds to voltage and heat flow to current, an established and documented approach that provides a clear and structured means of tracing heat flow through a system by assigning a thermal resistance to each component.

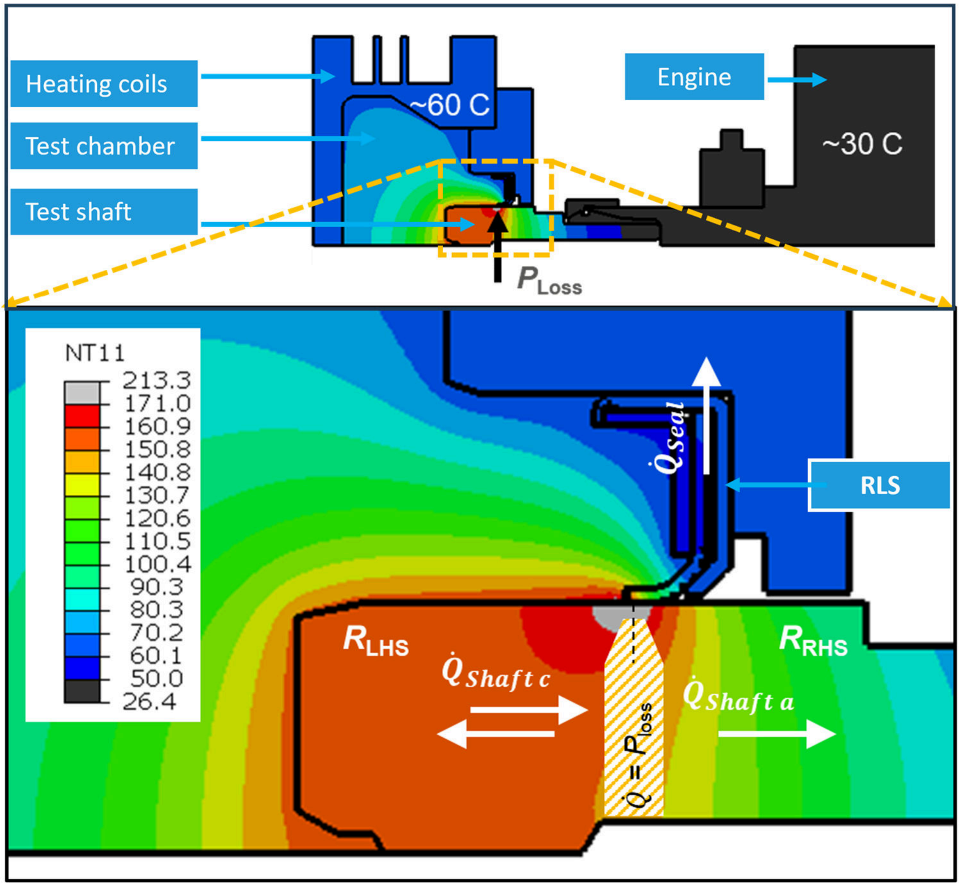

Figure 8: Thermal Model in ABAQUS representing SoS I test rig and representative thermal resistances in the system

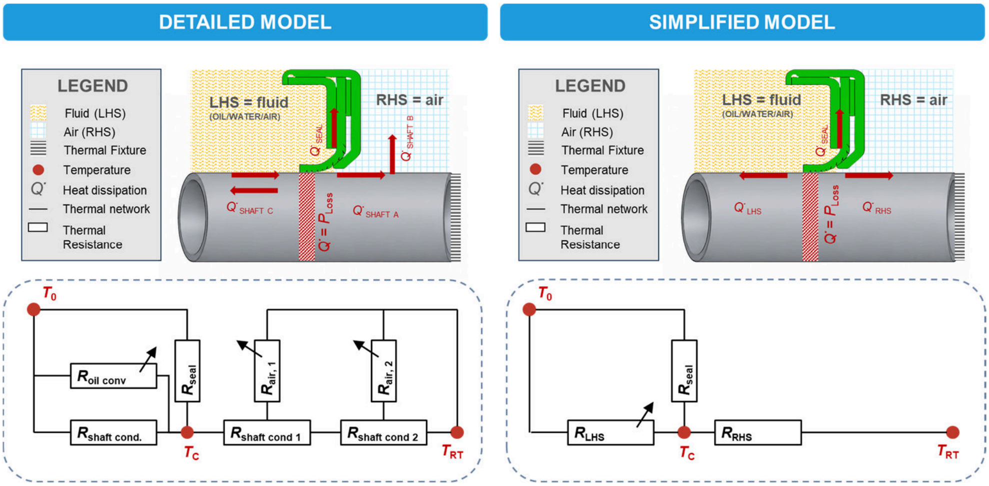

Figure 9: Detailed and Simplified Electrical Analogy Model as input for the Thermal Model

3.2.4 Data analysis

Simulation output is only as valid as the model it derives from, and FEA results should always be approached critically, questioning at each stage whether the boundary conditions and model setup adequately represent the physical test configuration.

In ABAQUS, temperatures are resolved at individual nodes across the mesh. Rather than extracting the temperature at a single node point, which is sensitive to local mesh effects and may not be representative due to steep thermal gradients, a mean value is computed across a set of nodes spanning a small region corresponding to the physical measurement area. This is directly motivated by the thermocouple geometry described in Section 3.1.1: with a tip diameter of 0.3 mm and a bore diameter of 0.8 mm. Nodal averaging over the equivalent region is therefore the appropriate extraction method and is applied consistently to T_{M1} at both, 0 mm and -1 mm.

Each model output is specific to a fixed set of system variables: shaft diameter, geometry, material, fluid type, fill level and initial sump temperature. Results are expressed as power loss against contact temperatures normalized by sump temperature, making them independent of seal design, radial load, shaft speed and pressure. This representation allows a given system configuration to be characterised once, and the output utilized across any combination of operating conditions and seal design to ensure the total power in the system remains within safe thermal limits.

As a further development, the model setup has been automated via a Python script that generates the geometry, mesh, boundary conditions and load definitions from a small set of input parameters. This significantly reduces the time required to analyse new configurations and is of value for high-speed bespoke applications where thermal margins are tight and the risk of heat-driven failure is elevated.

3.3 Verification

Verification of the thermal model was carried out against the experimental datasets described in Section 3.1. Two shaft diameters were selected for the verification study: 30 mm and 52 mm; these were tested across a range of fluid environments: oil at fill levels of 10%, 33% and 50%, water, and dry running. This design space was deliberately chosen to span a broad range of thermal resistance conditions on the fluid side, providing a robust basis against which the model predictions could be assessed. The experimental datasets available were extensive, and the simulated outputs were generated to match each condition directly for comparison.

A deliberate decision was made not to introduce scaling factors into the model. Instead, thermal material properties verified independently against measurements are used throughout, with the intent that the model predicts contact temperatures from first principles across varying thermal resistance scenarios, within an acceptable margin of error (±10%).

Figure 10 presents the verification results directly, comparing predicted contact temperatures at the 1 mm offset location against the corresponding measured values for six cases spanning the design space described above. The scatter in the experimental data is represented by the standard deviation, shown both in the bar charts and summarised in the accompanying table above.

Simulation vs. Measurement – Verification Study

Case Study	FEA - TM1(-1)	Measured - TM1 (-1)	SD Spread (±)	Error [=(B-D)/D]
Units	(°C)	(°C)		
Oil 33% filled D52 2000 RPM	95.9	98.5	1.87	-2.7%
Oil 33% filled D52 10000 RPM	132.6	133.1	10.06	-0.3%
Oil 33% filled D30 10000 RPM	119.5	120.8	8.62	-1.1%
Water Filled D30 10000 RPM	100.9	95.2	1.25	6.0%
Dry Running D30 10000 RPM	197.2	199.8	20.66	-1.3%
Oil 33% filled D52 16000 RPM	145.2	146.7	10.94	-1.0%

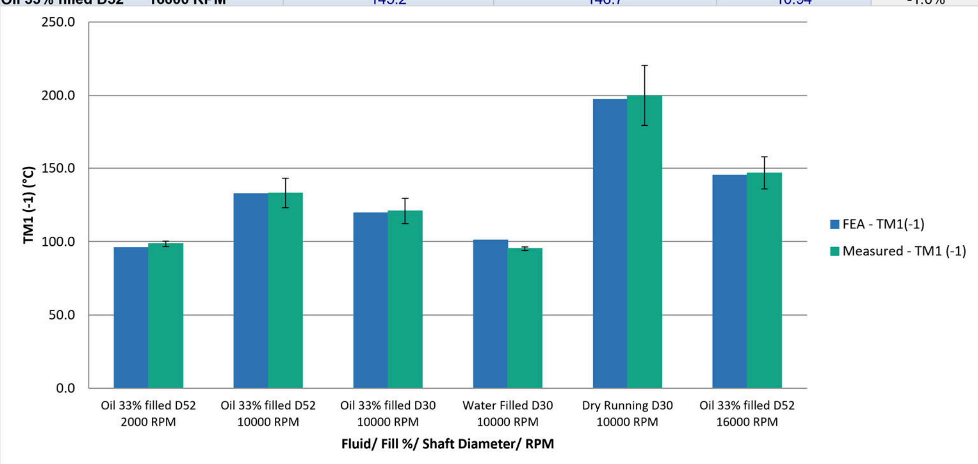

Figure 10: Contact Temperature (T_C respectively T_{M1}) Verification Study between Measurement and Prediction

4 Synopsis

To summarize, this work investigates the thermal behaviour of high-speed PTFE rotary lip seals, with a focus on predicting contact temperature as it has been identified a key driver of seal failure. A combined experimental and modelling approach was adopted to address the limitations of both standalone testing and purely theoretical simulations. Both approaches independently are insufficient.

An extensive experimental campaign was conducted using the SoS I high-speed test rig with carefully developed temperature measurement techniques, including an optimized embedded thermocouple method and infrared sensors along the shaft on the airside. The key development in the temperature measurement method from previous literature is the precise 1 mm offset from can be described as the 'local hottest zone'. The goal of this was focused on improving measurement repeatability, achieving linearity in the dataset and correctly interpreting local temperature gradients at the seal-shaft interface.

In parallel, a simplified yet physically representative thermal model was developed using finite element analysis in ABAQUS, supported by a reduced thermal resistance (analogy) framework. Key assumptions were made to achieve this such as negligible heat dissipation through the seal lip and lumped thermal resistances on the shaft sides. This was effectively to reduce the model complexity while retaining predictive capability.

The model was calibrated and verified against measured data across a wide range of operating conditions, including different shaft diameters, fluid types, and fill levels. Results demonstrate that the dominant factor governing contact temperature is the thermal resistance on the fluid side of the system.

Overall, the study shows that a well-calibrated, simplified framework can accurately predict contact temperatures (within ~±10%) provided that experimental data from physically accurate tests are utilized for verification. It is important to take note that accurate measurements are the key point for robust verification, made possible with the precise 1 mm offset measurement technique described. Thus, this combined experimental–numerical approach is essential: experimental data ensures real-world results and accuracy, while simulation enables scalability and broader applicability across configurations, providing practical insight into the dominant mechanisms controlling thermal performance in high-speed sealing systems.

5 Nomenclature

Variable	*Description*	*Unit*
T_O	Sump Temperature	°C
T_C	Contact Temperature	°C
ΔT	Change in Temperature	°C
Q_T	Heat dissipated at the interface	J
R_T	Thermal Resistances	K/W
LHS	Left hand side	-
RHS	Right hand side	-
T_{IR}	Temperature Infrared sensor	°C
P_{LOSS}	Power Loss	W
T_{M1}	Temperature Sensor at T_C	°C
μ	Coefficient of friction	-
d	Shaft diameter	m
l	Length	m
k	Thermal Conductivity	W/m.K
A	Area	m^2
F_R	Radial Force	N

6 References

[1] Bock, Eberhard: “Shaft seal incorporates temperature sensor projecting into fluid retained by seal.” Patent application DE000019912135A1

[2] Day, K. & Salant, R.F. (1999): “Thermal Elastohydrodynamic Model of a Radial Lip Seal – Part I: Analysis and Base Results.” ASME J. Tribol., 121(1), 1–10. doi:10.1115/1.2833803

[3] Engelke, Tobias: „Einfluss der Elastomer-Schmierstoff-Kombination auf das Betriebsverhalten von Radialwellendichtringen.“ PhD Thesis, University of Hannover.

[4] Feldmeth, S.; Bauer, F.; Haas, W. (2016): “Multiscale Simulation of Conjugate Heat Transfer in Radial Lip Seals.” STLE Annual Meeting / IMA, Universität Stuttgart.

[5] Feldmeth S.; Christoph Olbrich; Frank Bauer: “Influence of Lubricants on the Thermal Behaviour of Rotary Shaft Seals.” 22nd ISC 2022

[6] Goelz, Jan: „Manschettendichtringe aus PTFE-Compounds.“ PhD Thesis, University of Stuttgart.

[7] Hajjam, M. & Bonneau, D. (2006): “Influence of the roughness model on the thermoelastohydrodynamic performances of lip seals.” Tribology International, 39(3), 198–205. doi:10.1016/j.triboint.2005.09.002

[8] Huang, X.; Liu, Z. & Zhang, H. (2020): “Mixed Thermo-Elastohydrodynamic Lubrication Analysis of Rotary Lip Seals.” Proc. IMechE Part J: J. Eng. Tribology. doi:10.1177/0036850419881902

[9] Kang, Y.S. & Sadeghi, F. (1997): “Numerical Analysis of Temperature Distribution at the Lip Seal-Shaft Interface.” ASME J. Tribol., 119(2), 273–278. doi:10.1115/1.2833188

[10] Lines, D.J.; Lawrie, J.M.; O’Donoghue, J.P.: “Effect of Under-Lip Temperature on the Lubrication of Rotary Shaft Garter Spring Seals.” Proceedings of the Institution of Mechanical Engineers 181 (1966), Issue 9, p.185–190

[11] Maoui, A.; Hajjam, M. & Bonneau, D. (2008): “Analysis of Three-Dimensional Non-Axisymmetric Elastic Effects on TEHD Radial Lip Seal Behaviour.” ASME J. Tribol., 130(1), 012003. doi:10.1115/1.2842294

[12] Nomikos, P.; Rahmani, R. et al. (2024): “Analytical Thermal Network Model for Radial Lip Seal Contact Temperature Prediction.” Proc. IMechE Part D: J. Automobile Engineering. doi:10.1177/09544070231213903

[13] Stakenborg, M.J.L. & van Ostayen, R.A.J. (1989): “Radial lip seals, thermal aspects.” Leeds-Lyon Symposium on Tribology. doi:10.1016/S0167-8922(08)70183-4

[14] Thielen, S. (2019): “Entwicklung eines TEHD-Tribosimulationsmodells für Radialwellendichtringe.” PhD Thesis, TU Kaiserslautern, ISBN 978-3-95974-120-0.

[15] Upper, G. (1968): “Dichtlippentemperatur von Radial-Wellendichtringen – Theoretische und experimentelle Untersuchung.” PhD Thesis, University of Karlsruhe.

[16] Wennehorst, Bengt: “Lubrication and Friction in soft sliding contacts.” PhD Thesis, University of Hannover.

[17] Wollesen, Volkert-Martin: „Temperaturbestimmung in der Dichtzone von Radialwellendichtringen als Randbedingungen für die Modellierung des Dichtvorganges.“ PhD Thesis, TUHH.

7 Authors

Saint-Gobain Omniseal Solutions
Heiveldekens 9, 2550 Kontich, Belgium

Dr. Mirco Gronitzki, ORCID 0009-0001-8105-1613
mirco.gronitzki@saint-gobain.com

Dr. Sarah Shabbir, ORCID 0000-0003-1665-2487
sarah.shabbir@saint-gobain.com

https://doi.org/10.61319/NTCLZBNI